The crack path growth in aluminium alloy rectangular specimens under proportional bending with torsion

Dariusz Rozumek and Ewald Macha[1]

[1] Opole University of Technology, ul. Mikołajczyka 5, 45-271 Opole, Poland
e-mail: drozumek@po.opole.pl and emac@po.opole.pl

ABSTRACT. *The paper contains the results of investigations of the crack path growth in rectangular specimens made of the AlCuMg1 aluminium alloy under proportional bending with torsion loading. Specimens with rectangular cross-sections and stress concentrator in the form of external one-sided sharp notch were used. The tests were performed under the different ratios of torsion to bending moments and different stress ratio, R.*

INTRODUCTION

Under multiaxial loading, initiation of cracks and their development are usually evaluated according to classical strength hypotheses and stress crack growth criteria. They assume linear dependence between stresses and strains, and continuous medium. The well-known stress criteria using the stress intensity factor K for description of three crack modes have been formulated by Pook [1, 2] and Richard [3]. In practice, most machine elements are made of elastic-plastic materials, where plastic deformation can be observed. Thus, application of the criteria including such plastic changes (for example, the J-integral) seems to be the best solution. Sih [4] was one of the first researchers who had chosen energy approach (strain energy density) for description of the phenomena occurring while fatigue crack formation. He proposed a relationship describing the crack modes I and II. His analysis presented in [4] was based on tests of a plane disk subjected to simultaneous tension and shearing loading.

The aim of the paper is to describe fatigue crack growth rate in the aluminium alloy AlCuMg1 for different ratios of bending and torsional moments and different stress ratios, R.

EXPERIMENTS

The specimens were cut from the drawn aged bar, 16 mm in diameter. Dimensions of the specimens were the following: length $l = 90$ mm, height $b = 10$ mm and thickness $g = 8$ mm. The specimens had an external unilateral notch, 2 mm deep and with the rounding radius $\rho = 0.5$ mm [5]. The notches were cut with a cutter and their surfaces

were polished after grinding. Tests were performed under the constant moment amplitude M_a = 7.92 N·m and different stress ratios, R. Some mechanical properties of the tested aluminium alloy are given in Table 1.

Table 1. Mechanical properties of AlCuMg1 aluminium alloy

Yield stress σ_{YS} (MPa)	Ultimate stress σ_U (MPa)	Elastic modulus E (GPa)	Poisson`s ratio ν
382	480	72	0.32

The tests were realized on a fatigue test stand MZGS-100 where the ratio of torsion moment to bending moment was $M_T(t) / M_B(t) = \tan\alpha = \sqrt{3}/3, 1$ and $\sqrt{3}$ and loading frequency was 29 Hz. Crack development was observed on the specimen surface with the optical method. The fatigue crack increments were measured with a digital micrometer located in the portable microscope with magnification of 25 times and accuracy 0.01 mm. At the same time, a number of loading cycles N was written down. Fig. 1 shows a scheme of specimen loading [6].

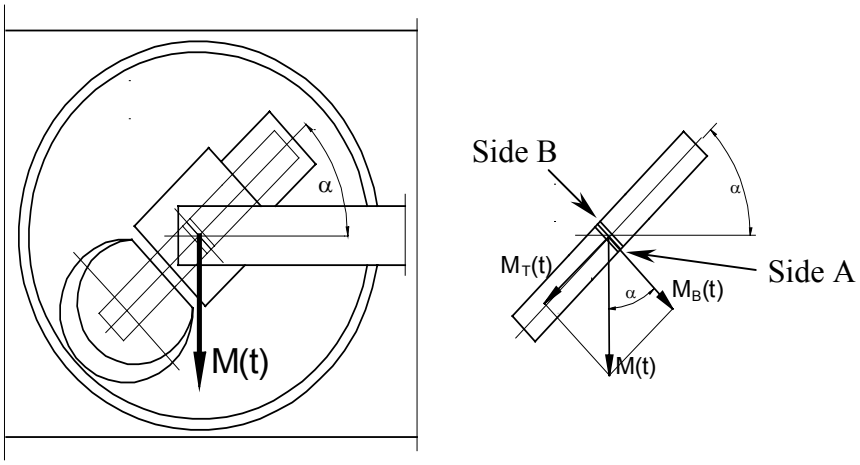

Figure 1. Loading of the specimen

THE TEST RESULTS AND THEIR ANALYSIS

Under proportional bending with torsion, fatigue tests were performed under controlled loading from the crack occurrence to specimen failure. The experimental results were shown as graphs of crack lengths a versus number of cycles N and crack growth rate da/dN versus ΔJ integral range. For calculations of stresses, strains, crack tip opening displacement and the J-integral, the computer programs FRANC2D and

FRANC3D were applied. Fig. 2 shows a typical crack path for AlCuMg1 aluminium alloy, occurring under mixed mode (I + III) loading.

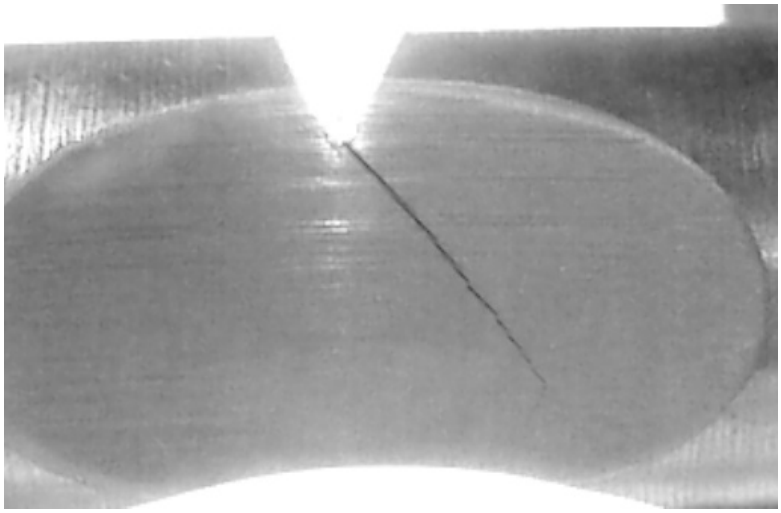

Figure 2. Crack development path under bending with torsion in AlCuMg1 alloy for R = - 1 and $\alpha = 60°$ (view of the side A), $N_f = 3.1 \cdot 10^5$ cycles

Cracks were initiated by the sharp notch. Macroscopic analysis of fractures (magnified ten times) based on visual inspection and photographs of the tested specimens was confronted with the dominating stresses in complex loading state (normal or shear). Fig. 2 shows the crack development path (side A) tested under the moment amplitude M_a = 7,92 N·m, the ratio of torsional moment to bending moment $M_T(t) / M_B(t) = \tan\alpha = \sqrt{3}$, the stress ratio R = - 1 and a number of cycles to failure $N_f = 3{,}1 \cdot 10^5$. In this case, the crack growth in the plane of maximum shear stresses. Similar behaviour of the same material was observed under the moment ratio $M_T(t) / M_B(t) = \tan\alpha = 1$. In the case of $M_T(t) / M_B(t) = \tan\alpha = \sqrt{3}/3$, the fracture plane inclination approached the plane of maximum normal stresses. During tests, non-uniform increment of crack length was observed at both sides of specimens, i.e. in front - side A and at the back – side B (similar behaviour was also observed in the case of application of the finite element method). In the side A crack lengths were a little greater than in the side B. Some typical results of calculations according to the boundary element method with the program FRANC3D are shown in Fig. 3 as the maps of normal stresses along axis y. Crack lengths for the side A are assumed for calculations, because they strongly influence failure of specimens. The stress fields in the side A are also greater than those in the side B of the specimen surface. From Fig. 4 it appears that the fatigue fracture surface is initiated from the side A of the specimen section and develops as sectors of the arcs bowed in direction of the developing crack and displaces to the specimen centre.

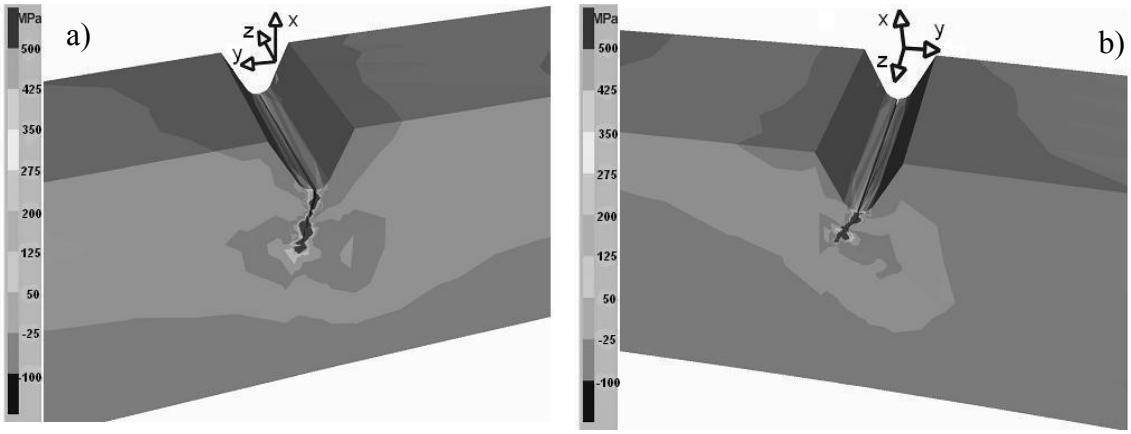

Figure 3. Distribution of normal stresses along axis y under bending with torsion M_a = 7.92 N·m (R = - 1) and crack length a = 2.15 mm, a) side A, b) side B

In Fig. 4 you can see a big fatigue zone and a small residual zone as well as beach marks. Fig. 5 shows fatigue crack growth versus number of cycles for different ratios of the torsional moment to the bending moment and the stress ratios R = - 1, 0.

Figure 4. Surface of fatigue fracture of the specimen under bending with torsion in AlCuMg1 alloy for R = - 0.5, $\alpha = 45°$ and $N_f = 3.5 \cdot 10^4$ cycles

From the graphs in Fig. 5 it appears that changes of the angle α from 30^o to 60^o are accompanied by decrease of fatigue life of the specimens.

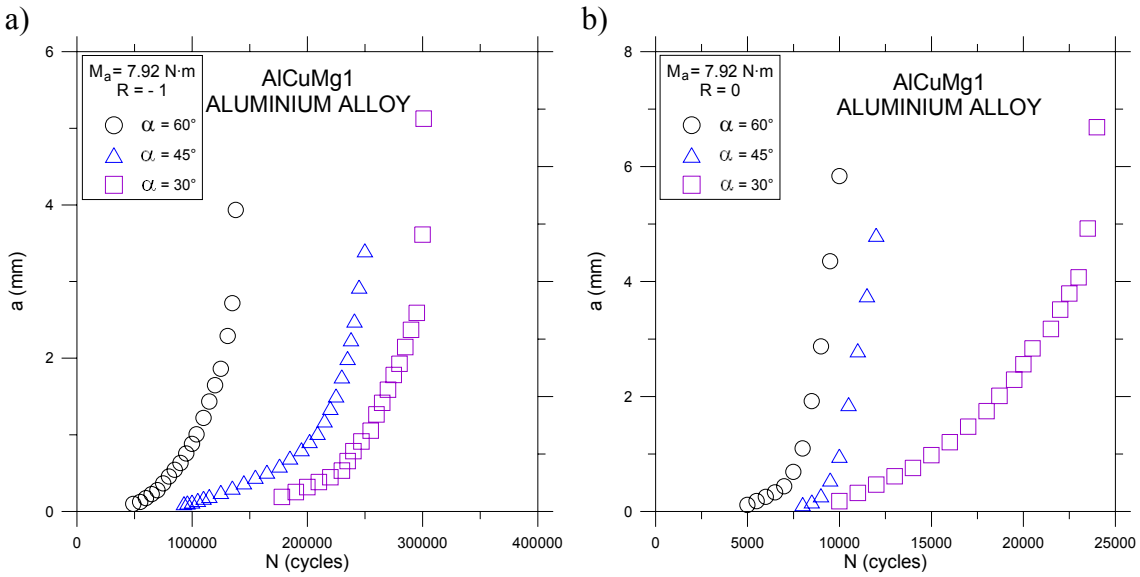

Figure 5. Fatigue crack growth versus number of cycles under mixed mode (I + III) loading for α = 30°, 45°, 60° and stress ratio a) R = - 1, b) R = 0

Figs. 6, 7 and 8 show crack growth rate da/dN versus ΔJ integral range for three angle α equal 30^o, 45^o, 60^o and the three stress ratios R = - 1, -0.5, 0. In these Figs. mixed modes I+III loading was separated into pure mode I and mode III. From Figs. 6-8 it appears that the cracking growth rate increases when we increase α from 30° to 60° in the aluminium alloy.

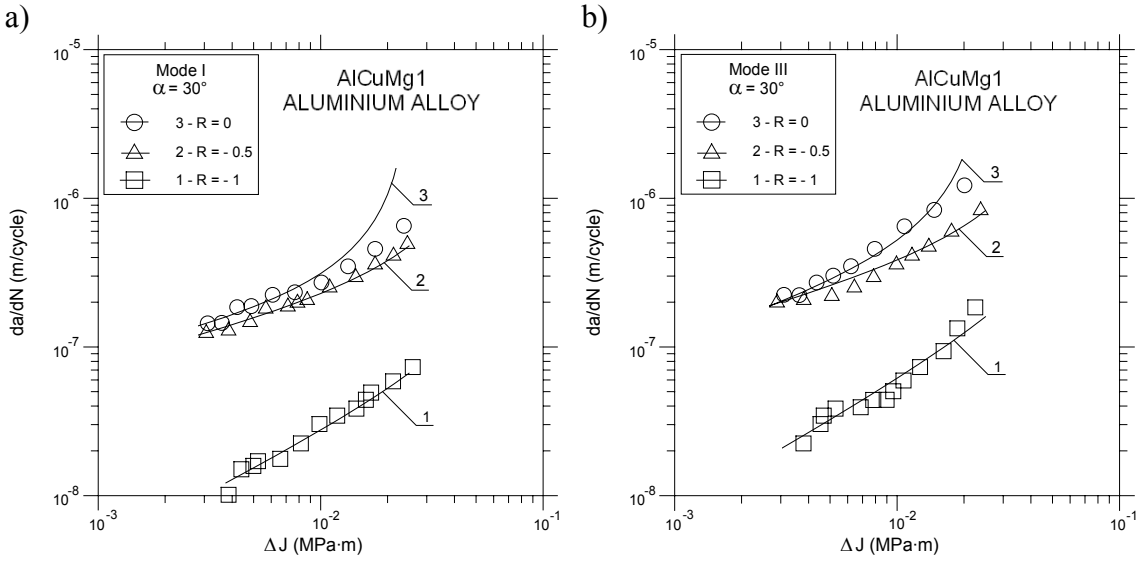

Figure 6. Comparison of experimental results for different stress ratios and α = 30° a) mode I, b) mode III

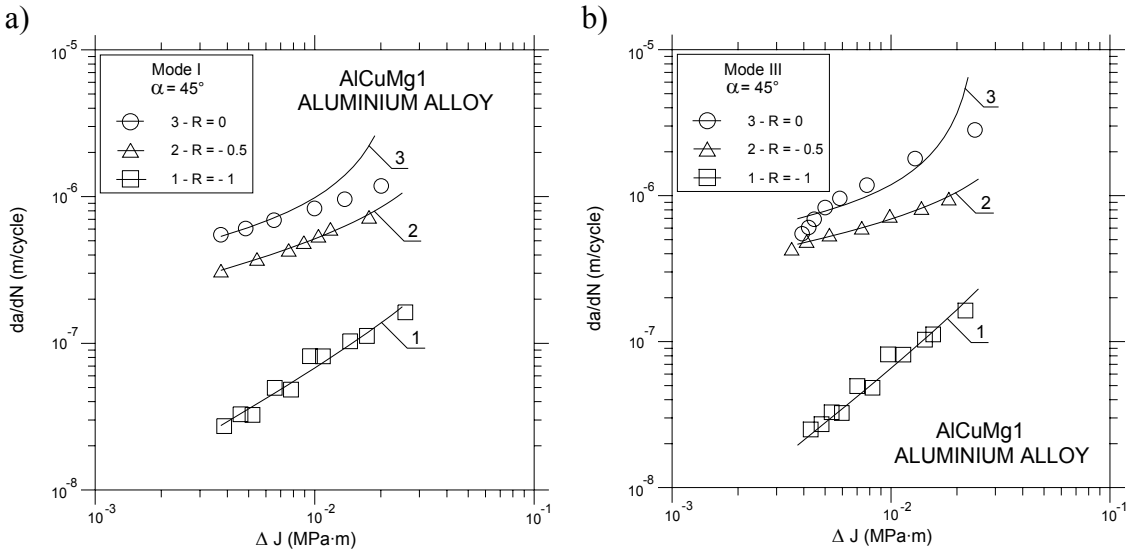

Figure 7. Comparison of experimental results for different stress ratios and α = 45° a) mode I, b) mode III

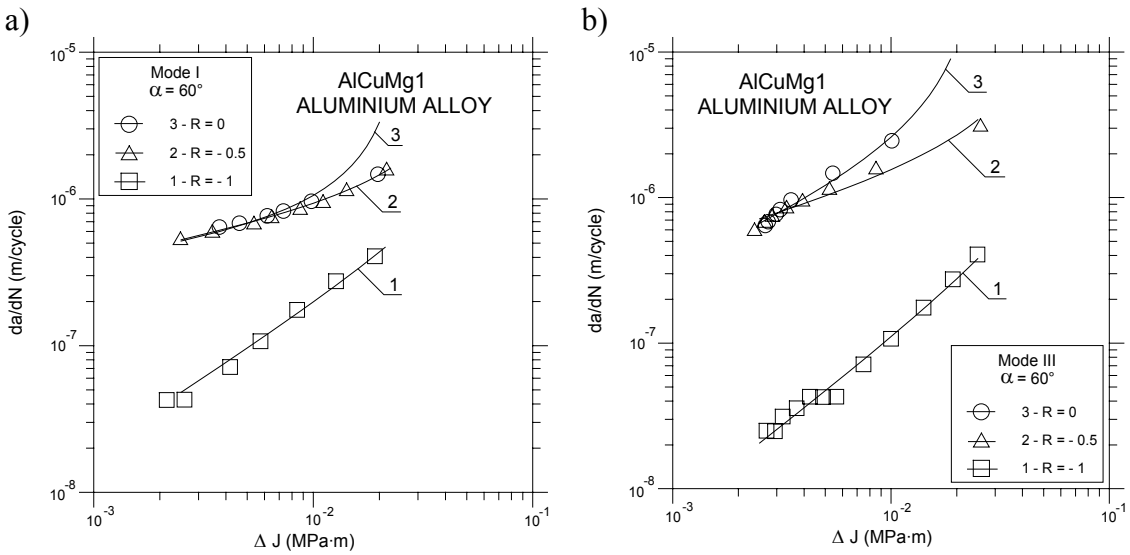

Figure 8. Comparison of experimental results for different stress ratios and α = 60° a) mode I, b) mode III

Moreover, we can state that for the stress ratio R = -1 and angle α = 30° the crack growth rate is higher for mode III than for mode I under the same value ΔJ; for angle α = 60° a higher rate is observed for mode I. For α = 45°, we observe a higher crack growth rate for mode I to da/dN = $8 \cdot 10^{-8}$ m/cycle (Fig. 7), above which mode III is dominating together with increase of the material plasticity. For R = - 0.5 and 0, for all

the considered angles α we can observe a higher crack growth rate for mode III. The experimental results shown in Figs. 6 to 8 for II and III range of crack growth rate were described with the following model [6]

$$\frac{da}{dN} = \frac{B\left(\frac{\Delta J}{J_0}\right)^n}{(1-R)^2 J_{Ic} - \Delta J}, \tag{1}$$

where J_{Ic} – critical value of the J-integral, $\Delta J = J_{max} - J_{min}$, $J_0 = 1$ MPa·m - unit value of the J-integral, B and n – coefficients determined experimentally.
The ΔJ integral range for mode I and mode III is calculated from

$$\Delta J_I = (1-\nu^2)\Delta K_I^2 / E + \pi M_{k1}^2 a\left(\Delta\sigma\Delta\varepsilon_p / \sqrt{n'}\right), \tag{2}$$

$$\Delta J_{III} = (1+\nu)\Delta K_{III}^2 / E + \pi M_{k3}^2 a\left(\Delta\tau\Delta\gamma_p / \sqrt{n'}\right), \tag{3}$$

where a – crack length, E – Young's modulus, ν - Poisson's ratio, n' - cyclic strain hardening exponent, ΔK_I, ΔK_{III} - stress intensity factors ranges for mode I and mode III, M_{k1}, M_{k3} - correction coefficients for mode I and mode III [6], $\Delta\sigma$, $\Delta\tau$ - ranges of stress under bending and torsion in the notch root, respectively, $\Delta\varepsilon_p$, $\Delta\gamma_p$ – ranges of plastic strains under bending and torsion in the notch root, respectively.
The empirical coefficients B and n occurring in Eq. (1) were calculated with the least square method and they were shown in Table 2.

Table 2. Coefficients B, n Eq. (1) and correlation coefficient r for the curves in Figs. 6 - 8

Figs., Graphs	B $\frac{MPa \cdot m^2}{cycle}$	n	r	Figs., Graphs	B $\frac{MPa \cdot m^2}{cycle}$	n	r
Fig. 6a-3	$0.31 \cdot 10^{-7}$	0.35	0.99	Fig. 6b-3	$0.80 \cdot 10^{-7}$	0.49	0.99
Fig. 6a-2	$0.70 \cdot 10^{-7}$	0.40	0.99	Fig. 6b-2	$1.31 \cdot 10^{-7}$	0.43	0.99
Fig. 6a-1	$0.91 \cdot 10^{-7}$	0.77	0.99	Fig. 6b-1	$2.30 \cdot 10^{-7}$	0.81	0.99
Fig. 7a-3	$0.57 \cdot 10^{-7}$	0.28	0.98	Fig. 7b-3	$0.50 \cdot 10^{-7}$	0.21	0.97
Fig. 7a-2	$1.42 \cdot 10^{-7}$	0.38	0.99	Fig. 7b-2	$1.22 \cdot 10^{-7}$	0.28	0.99
Fig. 7a-1	$3.23 \cdot 10^{-7}$	0.85	0.99	Fig. 7b-1	$1.35 \cdot 10^{-6}$	1.17	0.99
Fig. 8a-3	$0.51 \cdot 10^{-7}$	0.24	0.98	Fig. 8b-3	$1.08 \cdot 10^{-6}$	0.71	0.99
Fig. 8a-2	$1.88 \cdot 10^{-7}$	0.31	0.99	Fig. 8b-2	$6.22 \cdot 10^{-7}$	0.46	0.99
Fig. 8a-1	$1.61 \cdot 10^{-6}$	0.97	0.99	Fig. 8b-1	$2.16 \cdot 10^{-6}$	1.16	0.99

It can be seen that for pure bending and pure torsion they take different values. It means that B and n are not dependent on a kind of the material only. The test results for cyclic bending with torsion include the error not exceeding 20% at the significance level α = 0.05 for the correlation coefficients r given in Table 2. The multiple correlation coefficients in all the cases take high values and it means that the parameters of Eq. (1) are well fit to description of experimental results.

CONCLUSIONS

From the performed tests under proportional cyclic bending with torsion of specimens made of AlCuMg1 aluminium alloy we can draw the following conclusions:

1. The applied empirical formula (1) including ΔJ integral range is good for description of fatigue crack growth rate tests in modes I and III.
2. It has been found that mode III has a higher crack growth rate than mode I in the tested material and stress ratio R = - 0.5, 0.
3. For stress ratio R = - 1 and $\alpha = 30°$ the fatigue crack growth rate is higher for mode III compared with mode I under the same value ΔJ. For $\alpha = 60°$, a higher rate is observed for mode I.
4. It has been found that a change of the stress ratio from R = -1 to R = 0 and angle α from 30^o to 60^o causes increase of the fatigue crack growth rate.

REFERENCES

1. Pook, L.P. (1980) The significance of mode I branch cracks for combined mode failure, Fracture and Fatigue, Elastoplasticity, Thin Sheet and Micromechanism Problems, Ed. By J.C. Radon, Pergamon Press, Oxford, 143-153.
2. Pook, L.P. (1985) Comments on fatigue crack growth under mixed modes I and III and pure mode III loading, Multiaxial Fatigue, ASTM STP 853, ed K. J. Miller and M. W. Brown, American Society for Testing and Materials, Philadelphia, 249-263
3. Richard, H.A. (2003) Theoretical crack path determination, Int. Conf. on Fatigue Crack Paths, Ed. Carpinteri A., University of Parma, Parma, CD-ROM, 8ps.
4. Sih, G.C. (1974) Strain-energy density factor applied to mixed-mode crack problems, Int. Journal of Fracture, **10**, 305-321.
5. Macha, E., Rozumek, D. (2004) Fatigue crack growth in 18G2A steel under mixed modes loading I+III, Proc. of the 15th European Conference of Fracture, Advanced Fracture Mechanics for Life and Safety Assessments (ECF15), Stockholm, Sweden, KTH, CD-ROM, 8ps.
6. Rozumek, D. (2004) Application of ΔJ integral range for fatigue crack growth rate in mixed-modes I and III, Proc. of the 7th Int. Conf. on Biaxial/Multiaxial Fatigue and Fracture (ICBMFF7), DVM Berlin, 489-494.